NOAA Level 2 CyGNSS Winds Algorithm Theoretical Basis Document v1.2

Compiled by the
OSWT at NOAA-NESDIS-STAR

April 07, 2022

AUTHORS:

Faozi Said (NOAA STAR/GST) – faozi.said@noaa.gov

Zorana Jelenak (NOAA STAR / UCAR) – zorana.jelenak@noaa.gov

Paul S. Chang (NOAA STAR) – paul.s.chang@noaa.gov

TABLE OF CONTENTS

LIST OF FIGURES AND TABLES

Page

1 Introduction

The Ocean Surface Winds Team (OSWT) at NOAA-NESDIS-STAR has produced and made available to the public the latest version, v1.2, of NOAA Level 2 CyGNSS winds. This product provides time-tagged, precision geolocated along-track average wind speed of non-overlapping 25 km x 25 km cells. The data is made available in NetCDF file format. Each file provides the daily global coverage from all eight CyGNSS spacecraft. Corresponding latitude and longitude variables, including several Level 1 parameters are also included in these files. This document provides a brief description of the version history for this product. A science algorithm overview is presented in section 3. Level 1 and Level 2 validation is included in section 4. Section 5 provides key information about data access, the use of the quality flag, and data file content.

2 Major version updates

Since November 2019, NOAA has released three major versions:

- The first released data version of the NOAA Level 2 CyGNSS winds was version 1.0, made accessible to the public in November 2019 [1] [2].
- Version 1.1 was released in September 2020 with one major revision, namely, the inclusion of sea surface wind retrievals when the CyGNSS star tracker flag is set. This data was originally excluded from v1.0, due to poor performance. An algorithm was subsequently developed in order to restore and preserve as many wind retrievals as possible while this flag is set. Details about this algorithm are provided in Section 3.
- Version 1.2 includes four major updates, namely
    - the inclusion of data associated to a spacecraft roll angle greater than |5°|
    - a high wind correction
    - a full revision of the quality flag
    - the inclusion of a wind speed sample error variable

Additional details of these updates are included in sections 3 and 5.

3 Science Algorithm Overview

Each CyGNSS spacecraft has the capability of processing up to four simultaneous specular reflections from the GPS satellite constellation, thanks to its port and starboard side antennas. This results in a series of ‘tracks’ instead of the more familiar orbital ‘swath grids’ provided from traditional scatterometers. For each specular point, a compressed delay-Doppler map (DDM) is generated with dimensions of 11-500Hz Doppler by 17-¼ chips delay bins. From each of these DDMs, the normalized bistatic radar cross section (NBRCS) is estimated using a

3-delay by 5-Doppler bins centered around the specular point [3]. Sea surface wind speed can then be inferred from the NBRCS. The NOAA CyGNSS wind product is derived from the v2.1 CyGNSS NBRCS [4], and makes use of the so-called track-wise σ° algorithm [5] which is described thereafter.

3.1 Along-track gridding

Depending on the incidence angle of specular reflection, the spatial resolution of the v2.1 CyGNSS NBRCS varies between 25 and 40 km^2 [3]. Since the DDM sampling rate is 2 Hz (it was 1 Hz prior to July 2019), the resulting spacing between adjacent samples is ~3 km (~6 km prior to July 2019). This results in an inevitable NBRCS overlap between adjacent samples. In order to increase independence between adjacent NBRCS samples, a gridding procedure is implemented on a track-wise basis: along each track, consecutive NBRCS falling within a 25 km grid cell are averaged as shown in Figure 3-1. As can be seen, overlaps between adjacent NBRCS are now greatly minimized. Note that samples with the 'Poor overall' quality flag set are excluded from the NBRCS averaging.

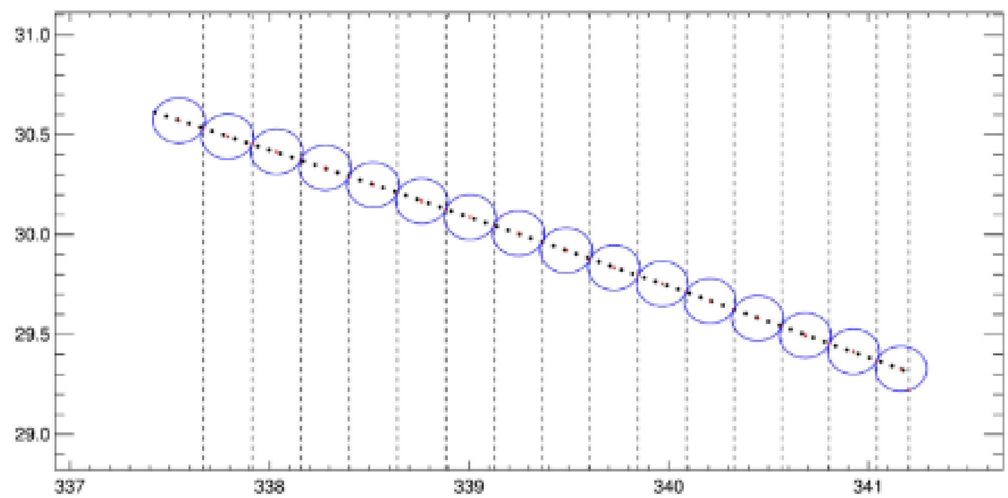

Figure 3-1 Plot showing geolocations of specular reflections along a CyGNSS track (see black dots). The NBRCS associated to all specular reflections found within each 25km blue circle are averaged, resulting in an along-track 25km gridded NBRCS

3.2 Boxcar averaging and track splitting

To further decrease noise in the NBRCS signal, a boxcar smoothing window is performed on the gridded NBRCS, using a window size of 3. Additionally, tracks may be split depending on the presence of gaps either due to samples triggering the poor overall quality flag, and/or when a given track is crossing a landmass. Justification for such track splitting is based on

noted NBRCS discrepancies when these gaps are present. The current condition in which tracks may be split is based on gaps longer than 10 seconds.
An additional track splitting scenario is also implemented, based on the along track receiver antenna gain: on longer gridded tracks (i.e. several hundreds of kilometers in length), the corresponding transect of the receiver antenna (Rx) gain pattern usually follows the shape of an inverse parabola. This usually results in areas of relatively low gain on both ends of the track. While degradation in the NBRCS has been noted in such cases, it has been difficult to find clear patterns. Consequently, such long tracks may be split at the peak of the along track Rx gain if and only if the original gridded track length is at least 1750 km, and each split track lengths are at least 500 km. The latter condition is used in order to prevent overfitting of the data.

3.3 Track-wise σ° bias correction

The track-wise σ° bias correction is necessary to address the residual calibration errors due to unknowns in the GPS transmitter and CyGNSS receiver chains that can yield significant errors [6]. The track-wise σ° bias correction requires the use of ancillary data such as from the ECMWF and HWRF models, as well as the IFREMER model significant wave height product [7]. The model datasets are initially bi-linearly interpolated to the version 2.1 CyGNSS NBRCS. Using the collocated NWP model winds and significant wave heights, including the incidence angle of specular reflection, the predicted along-track σ° is estimated using the NOAA geophysical model function. On a track-wise basis, a σ° bias is then computed between the predicted along-track σ° and the measured σ°. Note that the measured σ° samples used for the bias correction, must have an Rx gain greater than 3db and their collocated model winds fall within 35% of the tail of the along-track collocated model wind distribution.
This σ° bias is then used as a correction factor to the measured σ°, as shown in Figure 3-2. Note that this represents a single correction factor applied to all σ° along the whole track, thereby maintaining the 'shape' of the σ° timeseries.

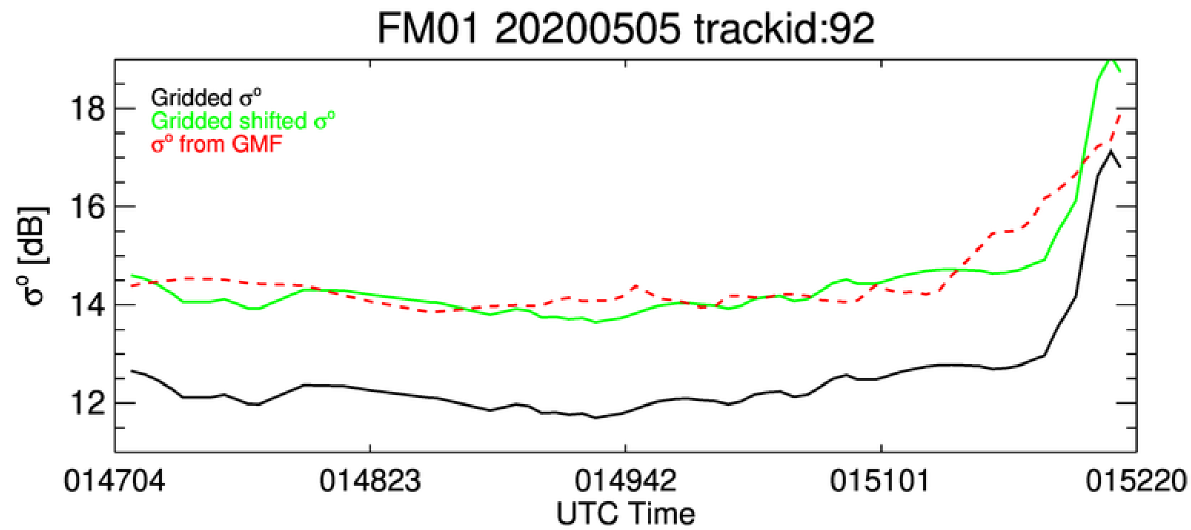

Figure 3-2 σ° timeseries from spacecraft 01 on 2020 May 05, track ID 92. The black curve shows the gridded σ° timeseries, while the green curve shows its shifted version using the track-wise σ° bias correction. The red curve shows the predicted σ° using collocated NWP model data. Note that the green curve is merely a shifted version of the black curve; its shape remains the same.

3.4 Wind speed retrieval

As shown in Figure 3-3, the NOAA GMF provides a relationship between σ°, the incidence angle, the wind speed, and the significant wave height. Using an *a priori* knowledge of the significant wave height and the incidence angle of specular reflection, a straightforward point-wise wind retrieval process is performed.

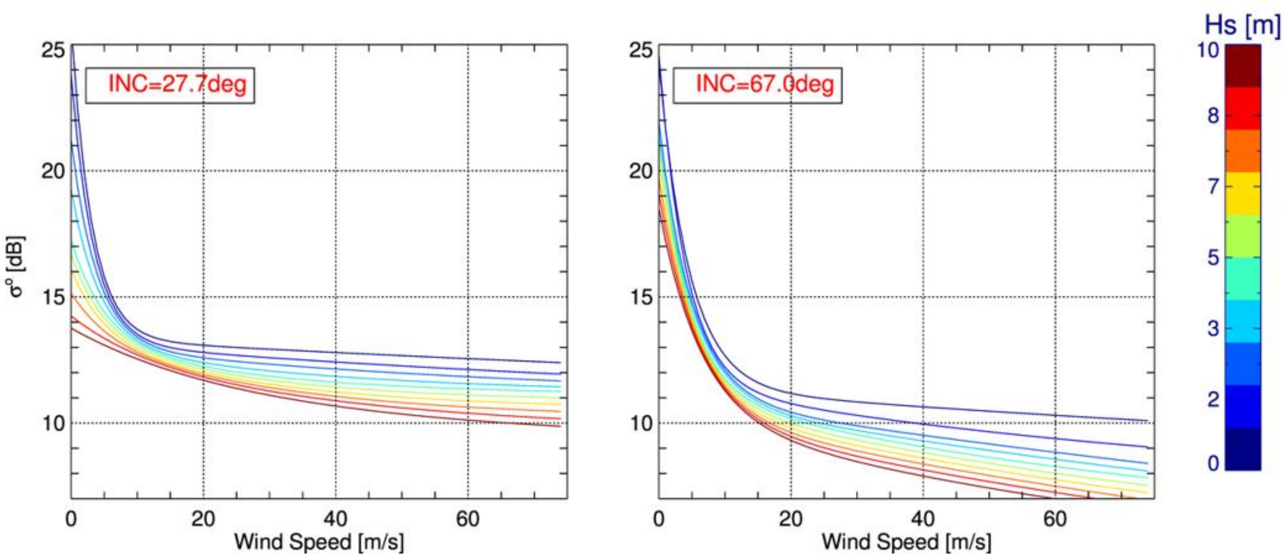

Figure 3-3 Plots illustrating NOAA geophysical model function providing the relationship between σ°, sea surface wind speed, the incidence angle of specular reflection, and the significant wave height. The left and right plots show such a relationship given a 27.7° and a 67° incidence angle, respectively.

Figure 3-4 shows the scatterplot of the retrieved CyGNSS wind corresponding to the σ° from FM#1 on May 2020 05 (track-id 92 – same track as shown in Figure 3-2). For perspective, this figure includes retrieved CyGNSS winds without the use of the track-wise σ° bias correction (see black samples).

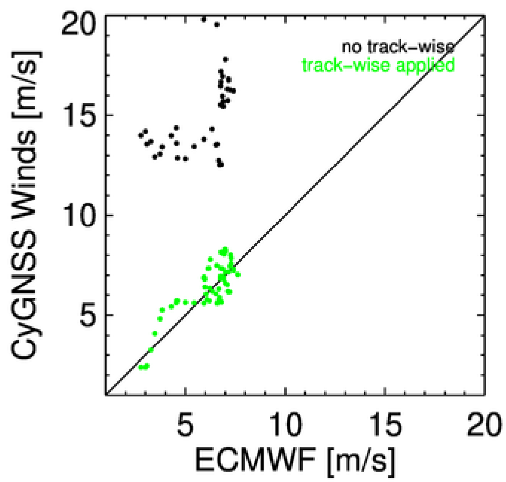

Figure 3-4 Scatterplot comparing NOAA CyGNSS winds against ECMWF with (green dots) and without (black dots) the track-wise σ° correction. Corresponding σ° were retrieved from track-id 92 from FM# 1 on May 2020 05 (see Figure 3-2).

3.4.1 Improving retrieval performance in the higher wind regime

As previously mentioned, the track-wise sigma0 bias correction algorithm makes use of collocated model winds in order to estimate predicted sigma0. It is important to note that the performance of the retrieved wind greatly depends on the performance of the collocated model winds utilized. As such, two adjustments are made to the model wind so as to improve CyGNSS high wind performance. First, a cumulative distribution function (CDF) matching technique is implemented in order to 'boost' ECMWF winds in the higher wind regime. To do so, ¼° ECMWF winds are collocated to ¼° HWRF winds for all available tropical cyclone overpasses within the Atlantic and eastern Pacific basins for the 2017 May to 2020 November period.

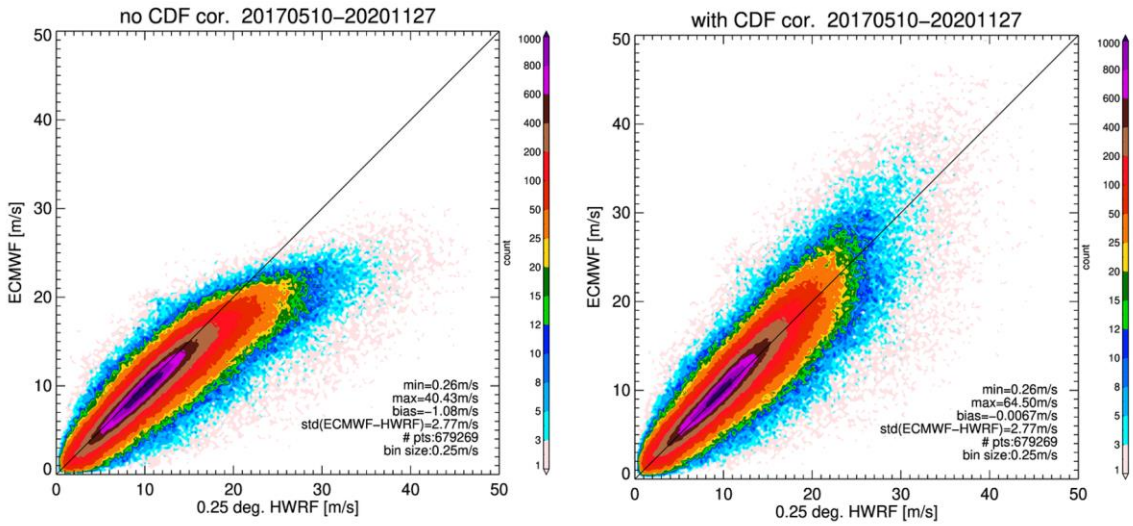

Figure 3-5 2-D histograms comparing ECMWF winds against collocated HWRF winds with and without the CDF matching correction applied. Without it (see left plot), ECMWF winds tend to underestimate the wind speed, when HWRF winds are greater than ~20 m/s. The CDF matching correction helps the scatter better align along the 1-1 line for the whole wind speed range, thereby decreasing the overall wind speed bias from -1.08 m/s to -0.01 m/s.

Figure 3-5 compares ECMWF to HWRF winds with and without the CDF matching correction. Without correction (see left plot), ECMWF tends to underestimate the wind when HWRF is greater than ~20 m/s. Once the correction is applied, the scatter now better aligns along the 1-to-1 line where the overall wind speed bias has decreased from -1.08 m/s to -0.01 m/s.
The second adjustments made to the model winds, used as an input to the track-wise sigma0 algorithm, is the use of a 'blended' model wind, where CDF corrected ECMWF winds are replaced with HWRF forecast winds whenever the latter are made available. These two considerations improve v1.2 NOAA CyGNSS winds in the higher wind regime. Section 4 will expand on the actual performance enhancements.

3.4.2 Quality control

Several algorithms are implemented so as to remove as many poor wind speed samples while minimizing overall data loss. This subsection provides a description of each of these algorithms.

3.4.3 Preretrieval QC

There are two main preretrieval filters applied to the data. First, it has been noted [5] that the quality of the measured σ° noticeably deteriorates when either the Rx gain or the SNR decreases. As a result, data meeting the following criteria are rejected:

$$(Rx \;\leq 3\ dB \wedge \mathrm{SNR} < 9\ \mathrm{dB}) \vee (\mathrm{SNR} < 1\ \mathrm{dB} \wedge \mathrm{Rx} < 7\ \mathrm{dB}).$$

Additionally, there are instances where σ° samples associated with the starboard side antenna have azimuth angles greater than 180° (starboard side azimuth angle ranges from 0 to 180°).

Conversely, there are instances where σ° samples associated with the port side antenna have azimuth angles less than 180° (i.e. port side azimuth angle ranges from 180 to 360°). Such samples are rejected, prior to performing the retrieval algorithm, given the fact that the antenna patterns are poorly characterized at these extreme azimuth angle ranges.

3.4.4 Post retrieval QC

3.4.4.1 Roll angle data

During high solar beta angle periods, each CyGNSS spacecraft roll angle is adjusted to maintain a power positive orientation [8]. As a result, the CyGNSS spacecraft roll angle was first adjusted to a positive or negative ~22° angle in the early stage of the mission, and subsequently adjusted to a positive or negative ~10° angle later on. In each case, however, wind retrieval performance suffers compared to when the roll angle is set to nadir. Figure 3-6 shows the median of the daily per-FM standard deviation of the error (stde) between CyGNSS and ECMWF per CyGNSS antenna for different spacecraft roll angles. As can be seen, the stde is noticeably higher whenever the spacecraft roll angle is away from 0°.

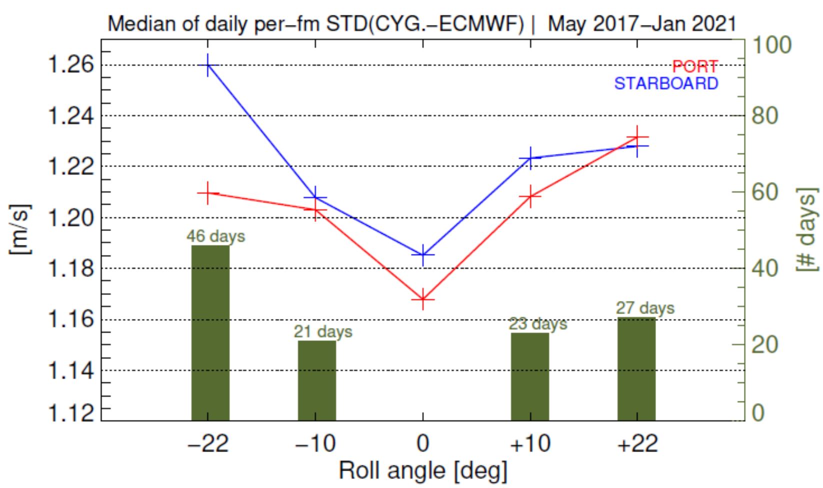

Figure 3-6 Plot reporting the median of the daily per-FM stde for a given spacecraft roll angle. The data is separated by CyGNSS antenna. As can be seen, the stde is smallest when the roll angle is close to 0°. The green bars report the number of days for which the roll angle was set to either +/-22° or +/-10°, simultaneously to all eight FMs.

Versions 1.0 and 1.1 of NOAA CyGNSS winds originally excluded such data. However, in v1.2 an algorithm is implemented in order to remove poor quality samples while minimizing the amount of flagged data. This algorithm makes use of a point-wise σ° bias computation between measured and predicted σ° values. If the absolute value of the bias exceeds a threshold of 1.35 dB, the corresponding retrieved wind sample is discarded. Additionally, samples meeting such criteria will only be flagged if several of them are found along a stretch greater than ~100 km. This condition is imposed to minimize the possibility of flagging areas where CyGNSS may detect ocean fronts and other microscale phenomena the model may miss.

Figure 3-7 shows the relationship between shifted σ° and collocated model winds (see green dots) from track-id 16 retrieved from spacecraft #2 on January 03 2018 where the roll angle was set to ~22°. Dots with red 'x' correspond to flagged samples.

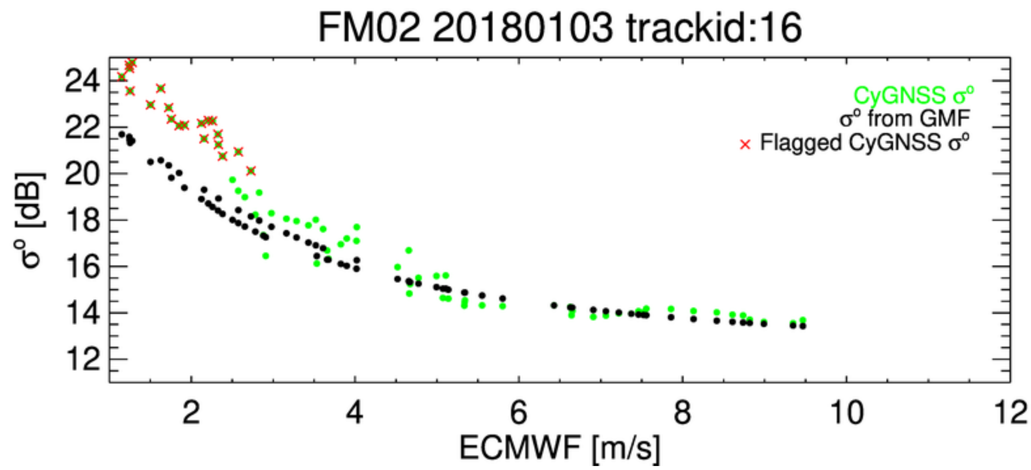

Figure 3-7 Plot showing the relationship between measured (see green dots) and predicted (see black dots) σ° versus collocated model wind. The red 'x's refer to samples flagged by the point-wise roll angle flagging algorithm.

3.4.4.2 Star tracker flag

A nano star tracker is being used by each CyGNSS satellite in order to provide accurate attitude knowledge. There are times when the star tracker is unable to view the stars, thereby decreasing the confidence in the reported attitude. The 'nst_att_status' flag variable (made available in the Level 1 NetCDF files) becomes non-zero whenever this occurs (see Figure 3-8 showing the daily percentage of data with this flag set).

To retain as many along-track samples as possible while the star tracker flag is set, a similar method, as described in 3.4.4.1, is implemented where a point-wise σ° bias between predicted and measured σ° is also computed. A specific threshold of 0.55 dB is selected where all samples above the absolute value of this threshold are rejected.

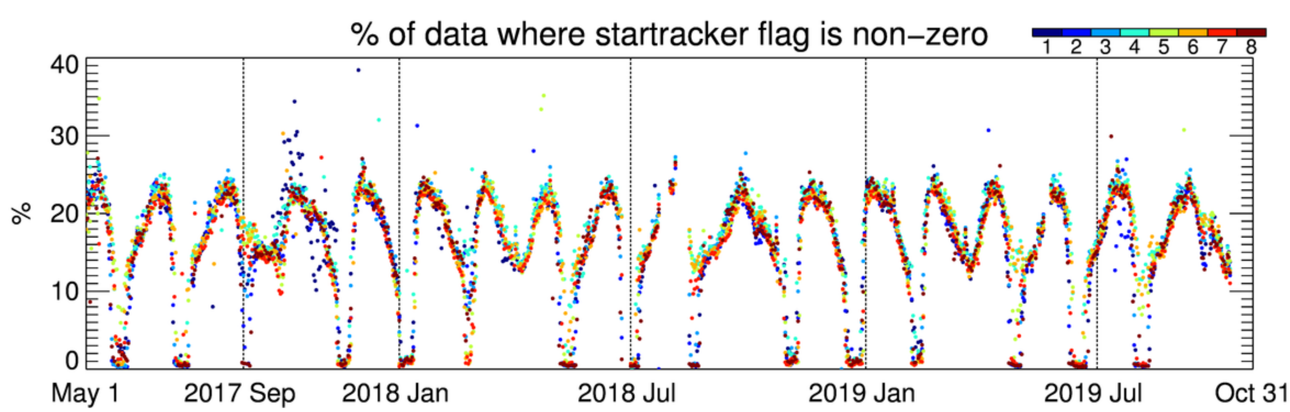

Figure 3-8 Timeseries reporting the daily percentage of CyGNSS data for which the star tracker flag was set. The percentage values are separated by CyGNSS spacecraft.

3.4.4.3 Tracks crossing 'Flex power' events

The transmitted power levels from blocks IIF and IIR-M have been intermittently changed since January 2017, and particularly after mid-February 2020, without user notice [9] [10]. Since most of these flex power events are regional, a CyGNSS track crossing such a region would exhibit a sudden and unpredictable change in σ° (see Figure 3-9). The current version of our track-wise retrieval algorithm is unable to compensate for such irregular shift in σ°. As such, an algorithm has been developed in order to detect tracks affected by flex power events, by monitoring the rate of change of the noise floor (dNF/dt) along each block IIF and IIR-M track. Whenever dNF/dt passes a preset threshold, the whole track is discarded.

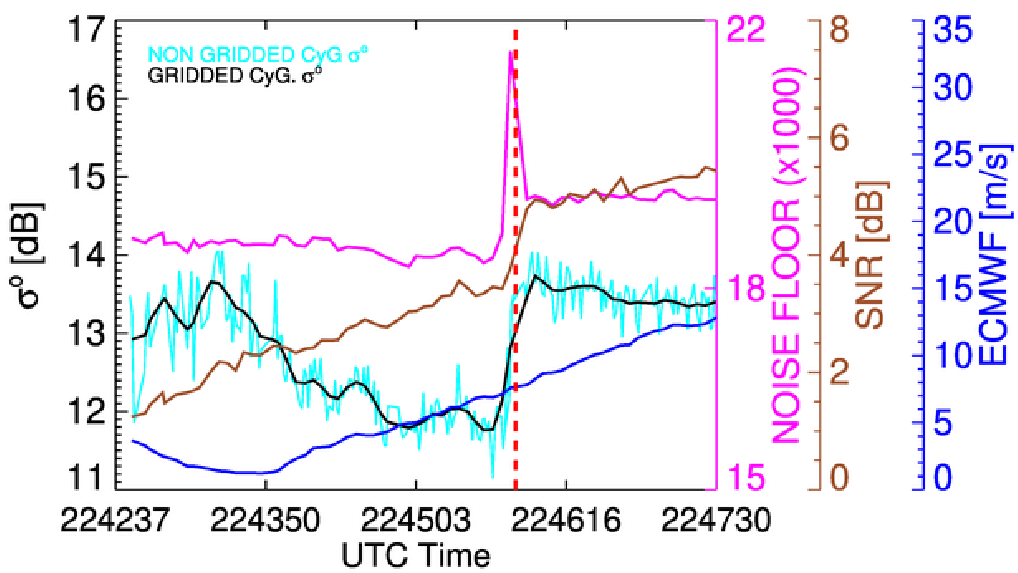

Figure 3-9 Gridded and non-gridded timeseries of CyGNSS σ° along track-id 846 retrieved from spacecraft #3 on 2017 July 30. Timeseries of noise floor and SNR quantities are also included. Note the sudden jump of these two quantities, including the σ°, as indicated by the vertical red dotted line. This sudden jump correlates with a geographical area where the GPS transmit power was drastically altered. Such a track is discarded.

3.4.4.4 Unrealistic wind speed sample flagging

Despite the use of our pre-qc flagging strategy, the presence of CyGNSS tracks reporting unrealistic retrieved wind speeds still exists. Figure 3-10 shows such an example where retrieved wind speeds from spacecraft #3 reported unrealistic wind speeds compared to neighboring tracks. Although not confirmed at this time, a possible reason for this problem is the effect of RFI.

An algorithm has therefore been developed in order to 'catch' and eventually flag these outlier samples. It first identifies all retrieved wind samples with an absolute bias, against collocated model wind, greater than 6 m/s.

Let s_{u10} represent a CyGNSS wind speed sample in m/s to be evaluated, and let mod_{u10} represent its collocated model wind speed sample. s_{u10} is then collocated with surrounding

CyGNSS wind samples within an 80 km radius and a 45-minute time window (see orange circle from Figure 3-10). If no sample is found, then the radius is extended to 240 km (see red circle from Figure 3-10), and the time window increased to 90 minutes. In both situations, s_{u10} is compared to the median of the collocated samples med_{u10}. Sample s_{u10} is then flagged using the following conditions:

- If (s_{u10}- mod_{u10}) < -6, then s_{u10} is flagged if s_{u10}- med_{u10} < -4
- If (s_{u10}- mod_{u10}) > 6, then s_{u10} is flagged if

$$(med_{u10} \leq 10 \ \wedge (s_{u10} - med_{u10}) > 10) \vee$$
$$(10 < med_{u10} < 15 \ \wedge (s_{u10} - med_{u10}) > 12) \ \vee$$
$$(med_{u10} \geq 15 \ \wedge (s_{u10} - med_{u10}) > 15).$$

If there is no collocated CyGNSS samples from either collocation scenario (i.e. orange or red circles from Figure 3-10), then s_{u10} is compared with its along-track adjacent samples. s_{u10} is flagged if its wind speed is greater than 25 m/s from its direct neighbors.

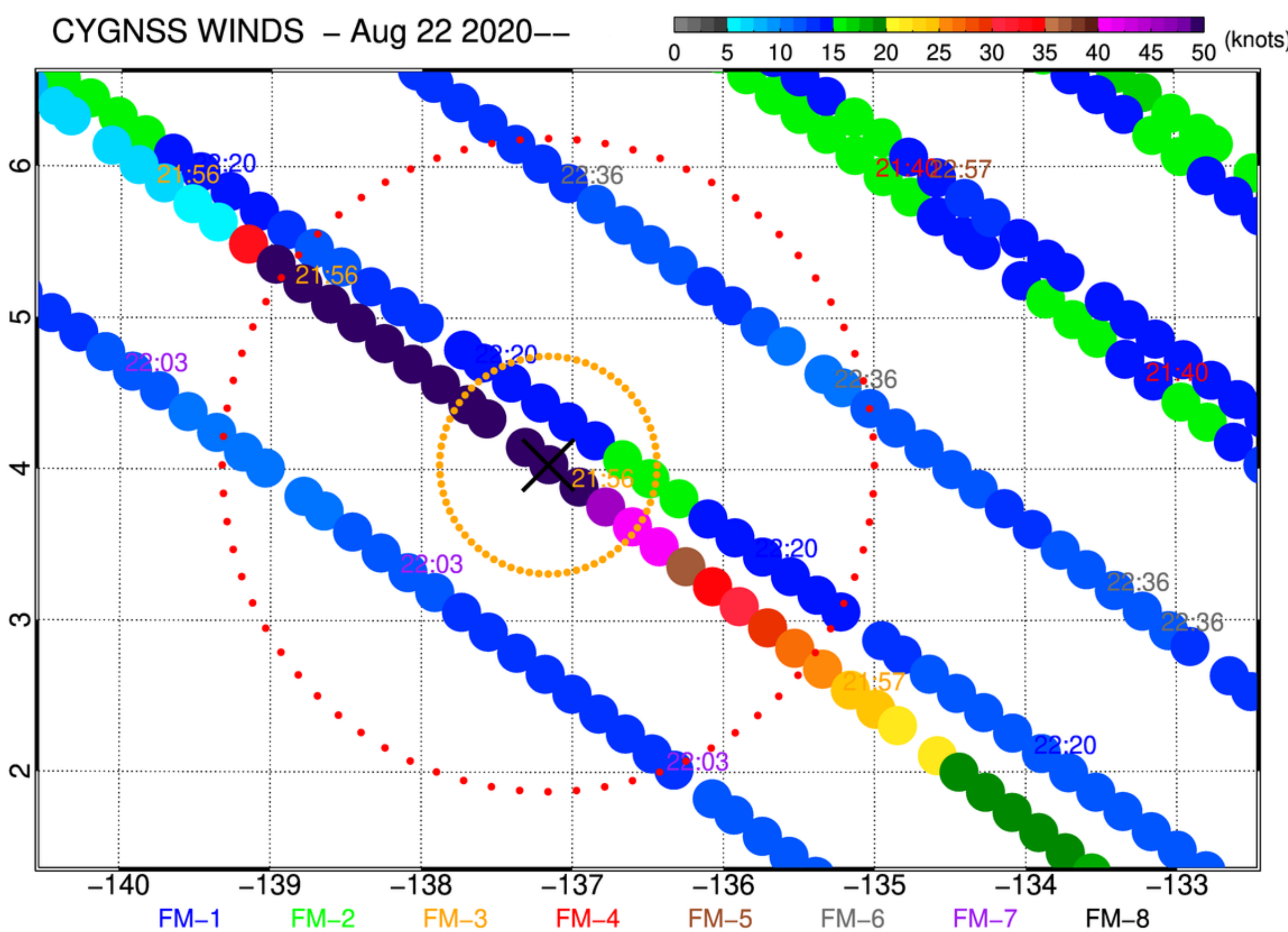

Figure 3-10 Example of an 'outlier track' where the reported wind speed deviates greatly from surrounding tracks from other spacecraft. Timestamps are provided along each track, and are color coded by CyGNSS spacecraft. The black 'X' is centered on an outlier sample which is compared against collocated samples within an 80 km radius (see orange circle) and a 45-minute time window, or a 240 km radius and a 90-minute window (see red circle) in case the first set of criteria fails to return any collocated samples.

3.4.4.5 Additional Filtering Strategy

An additional filtering method is also implemented in our wind retrieval algorithm (see Appendix B of [5]). This filtering strategy makes use of the wind speed error (i.e. retrieved – model) as a function of three sensor parameters, namely: the receiver antenna gain, the signal-to-noise ratio, and the incidence angle of specular reflection. An error probability P_{err} is then defined such that

$$P_{err} = \left(|U_{10}^{ret} - U_{10}^{mod}| > 2 \;\middle|\; \{SNR, Rx, \theta_i\}\right),$$

where U_{10}^{ret} represents CyGNSS retrieved wind samples, U_{10}^{mod} represents collocated model wind samples, SNR represents CyGNSS sample signal-to-noise ratio, Rx represents the receiver antenna gain, and θ_i represents the incidence angle of specular reflection.

This error probability look-up table is designed by collecting wind speed data from a four-month period (July to October 2017). The data is then separated using four ranges of incidence angle

$$\theta_i < 20°$$
$$20° \leq \theta_i < 40°$$
$$40° \leq \theta_i < 60°$$
$$\theta_i \geq 60°.$$

Within each incidence angle range, the data is then binned using a 0.15 dB bin size along both the Rx gain and SNR dimensions. Wherever the 2 m/s threshold is reached, the bin is then assigned a flag value of 1 (see Figure 3-11).

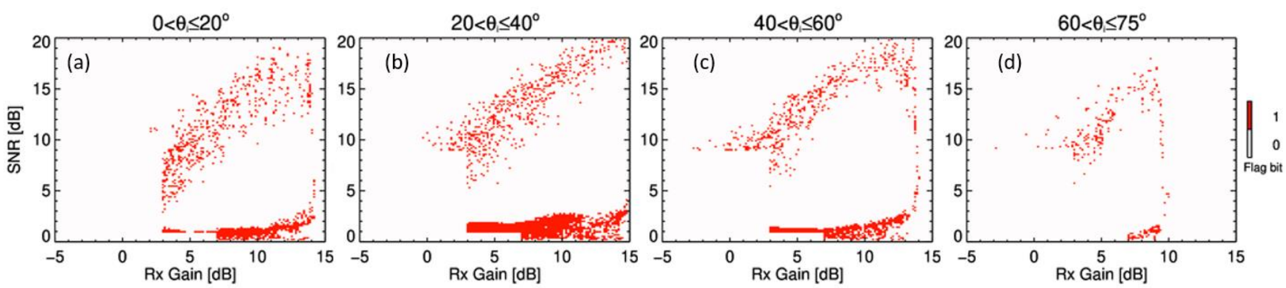

Figure 3-11 Plots showing the probability of the wind speed error being greater than 2 m/s, given the incidence angle of specular reflection, the SNR, and the receiver antenna gain. Each bin is 0.15X0.15 dB. A bin is assigned a flag bit value of 1 (see red color) whenever the 2 m/s wind speed error threshold is reached.

4 Validation

This section is divided into two main parts. The first portion covers the impact of the track-wise σ° bias correction on the CyGNSS σ° measurements. The second portion includes a series of analysis of v1.2 NOAA CyGNSS winds against model winds such as ECMWF and HWRF.

4.1 Track-wise σ° bias correction impact on CyGNSS σ°

4.1.1 Timeseries

σ° timeseries figures are an important means in identifying trends, biases, and possible remaining calibration issues in the measured signal. Given the fact that the CyGNSS constellation consists of eight small satellites, each equipped with two nadir antennas, and each receiving specular reflections from GPS satellites from three different block types, it is imperative to check for possible intersatellite σ° biases, biases between CyGNSS antennas, as well as possible σ° biases between different GPS block types. Figure 4-1 shows

- timeseries of daily averaged σ° (see plots a and b),
- daily averaged σ° with track-wise correction applied (see plots c and d)
- daily averaged σ° bias (i.e. $\sigma°_{measured}$-$\sigma°_{predicted}$ -- see plots e and f)
- daily averaged σ° bias with track-wise correction applied to the $\sigma°_{measured}$ (see plots g through j).

In this figure, the data is separated by CyGNSS antenna (i.e. for port side see plots a,c,e,g,i), and for starboard side see plots b,d,f,h,j) and spacecraft number (see figure legend). We first note that a decreasing σ° trend is present (see plots a and b). This trend is then removed thanks to the track-wise σ° correction (see plots c and d). The presence of intersatellite σ° biases, as well as σ° biases between a given spacecraft nadir antennas, is also noticeable when assessing the timeseries of uncorrected σ° biases (see plots e and f). The use of the track-wise σ° bias correction is able to greatly reduce these remaining calibration issues (see plots g and h, as well as a 'zoomed in' version of each --- see plots i and j).

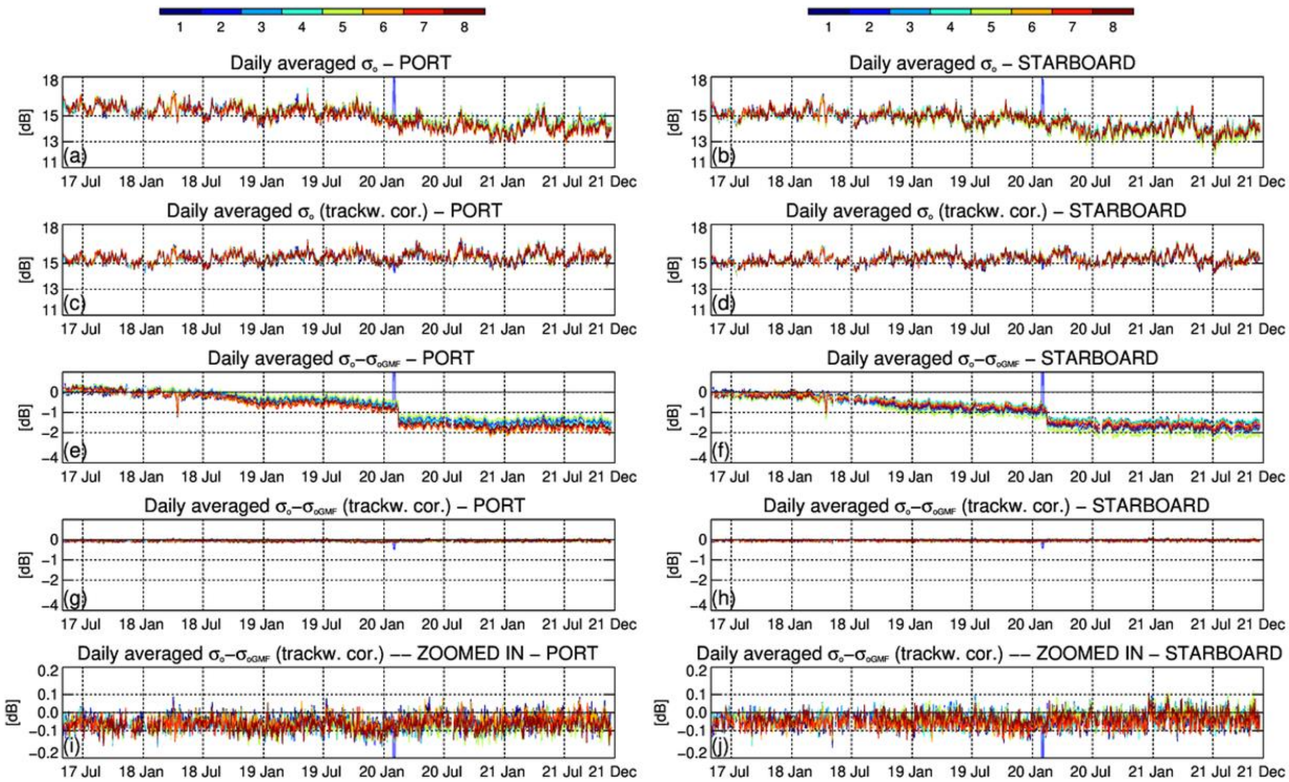

Figure 4-1 Daily averaged σ° timeseries separated by CyGNSS antenna and spacecraft number. The following metrics are presented in this figure: uncorrected daily averaged σ° (see plots a and b), track-wise corrected daily averaged σ° (see plots c and d), daily averaged σ° bias (i.e. measured-predicted) without and with track-wise correction applied (see plots e and f, and g and h, respectively). Note that plots i and j are 'zoomed in' version of plots g and h.

Similarly, Figure 4-2 reports the same metrics, namely

- the daily averaged σ° (see plots a and b)
- the daily averaged σ° with track-wise correction applied (see plots c and d)
- daily averaged σ° bias (i.e. $σ°_{measured}$-$σ°_{predicted}$ -- see plots e and f)
- daily averaged σ° bias with track-wise correction applied to the $σ°_{measured}$ (see plots g through j).

This time, the data is separated by CyGNSS antenna and GPS block type (see figure legend). The daily averaged σ° timeseries (see plots a and b) show a similar decreasing trend, as previously noted, with the addition of a major shift in σ° level for data associated to block IIR-M due to a flex power event noted in [10]. The track-wise bias correction algorithm is able to remove this noted shift, as shown in plots c and d. Similar observations are made when comparing daily averaged σ° biases without and with track-wise correction (see plots e through j).

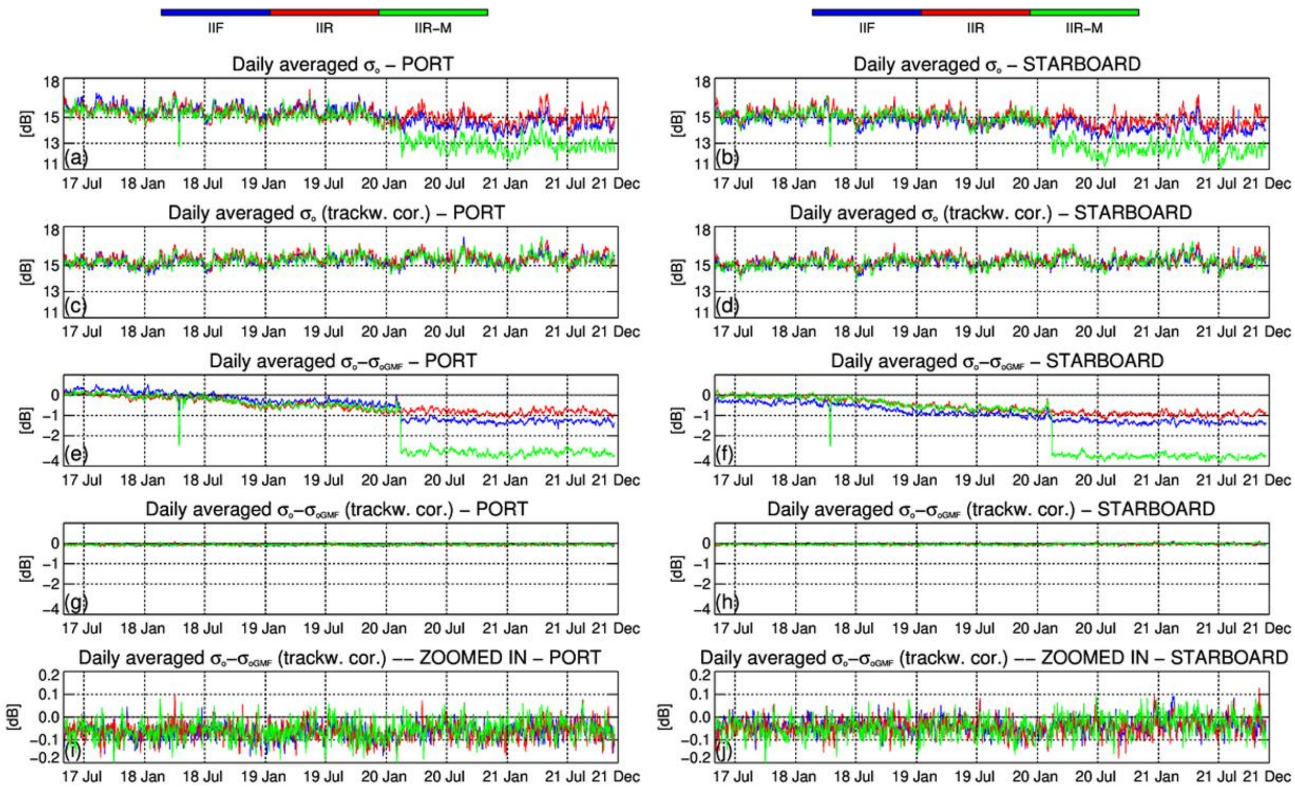

Figure 4-2 Daily averaged σ° timeseries separated by CyGNSS antenna and GPS block type. The following metrics are presented in this figure: uncorrected daily averaged σ° (see plots a and b), track-wise corrected daily averaged σ° (see plots c and d), daily averaged σ° bias (i.e. measured-predicted) without and with track-wise correction applied (see plots e and f, and g and h, respectively). Note that plots i and j are 'zoomed in' version of plots g and h.

4.1.2 Spatial distribution of the σ° bias correction

The track-wise σ° bias correction is now plotted on a map so as to assess its geographical distribution. The data is separated by GPS block type, CyGNSS antenna and orbital node (see Figure 4-3 for the ascending node and Figure 4-4 for the descending node). In these two figures, the selected time period is May 01 2017 to February 01 2020, thereby excluding the major flex power event applied to block IIR-M data. The most notable bias correction patterns in these figures are those associated to flex power events applied throughout the whole time period to block IIF data (see plots a and b from both Figure 4-3 and Figure 4-4).
Figure 4-5 shows the track-wise σ° bias correction for block IIR-M only for the March-November 2020 period, highlighting the changes in bias correction level and geographical pattern once the mid-February 2020 flex power event was implemented. Figure 4-6 and Figure 4-7 show how the bias correction levels and geographical patterns have changed for blocks IIF and IIR for that same time period. These level changes correlate with the noted decreasing σ° trend from Figure 4-1 (see plots a and b), where σ° from both blocks IIF and IIR slowly decreased overtime, resulting in the need of increased bias correction.

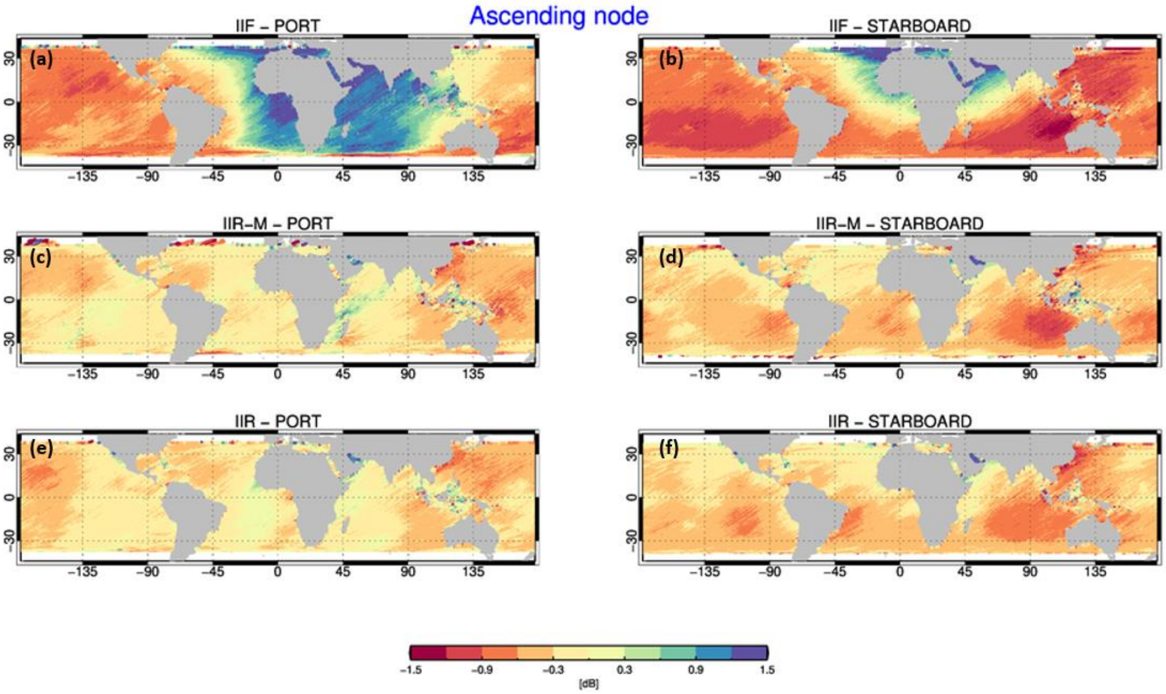

Figure 4-3 Track-wise σ° bias correction for CyGNSS ascending node plotted on a map, separated by GPS block type and CyGNSS antenna, for the May 01 2017-Feb 01 2020.

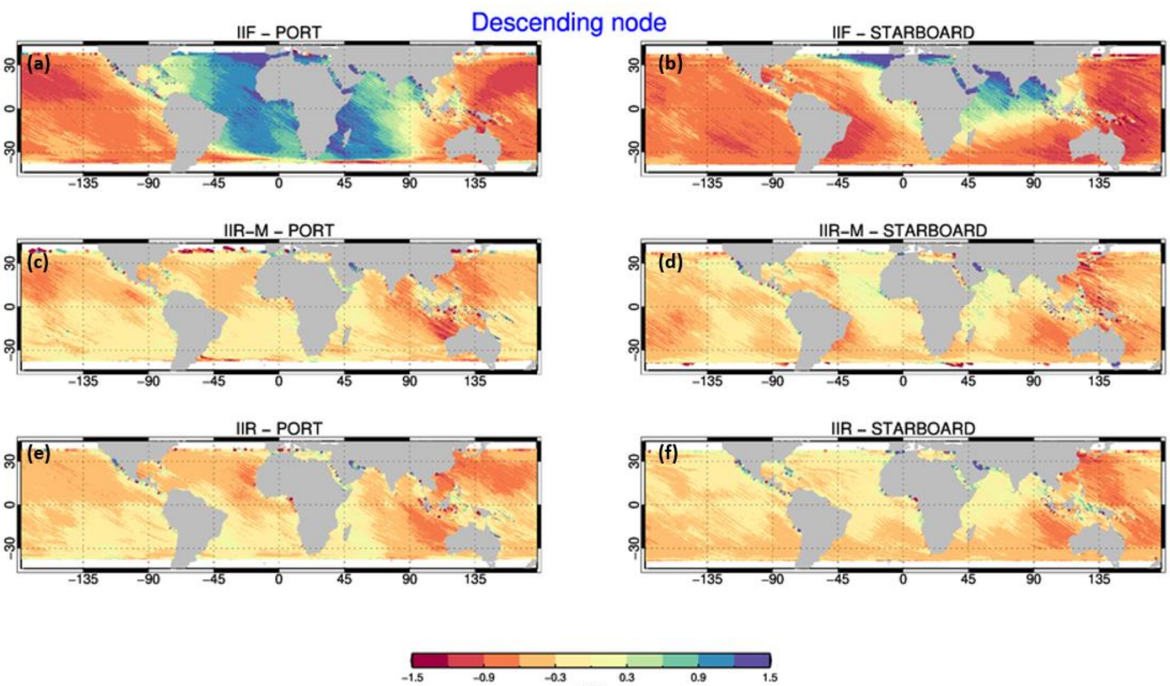

Figure 4-4 Track-wise σ° bias correction for CyGNSS descending node plotted on a map, separated by GPS block type and CyGNSS antenna, for the May 01 2017-Feb 01 2020.

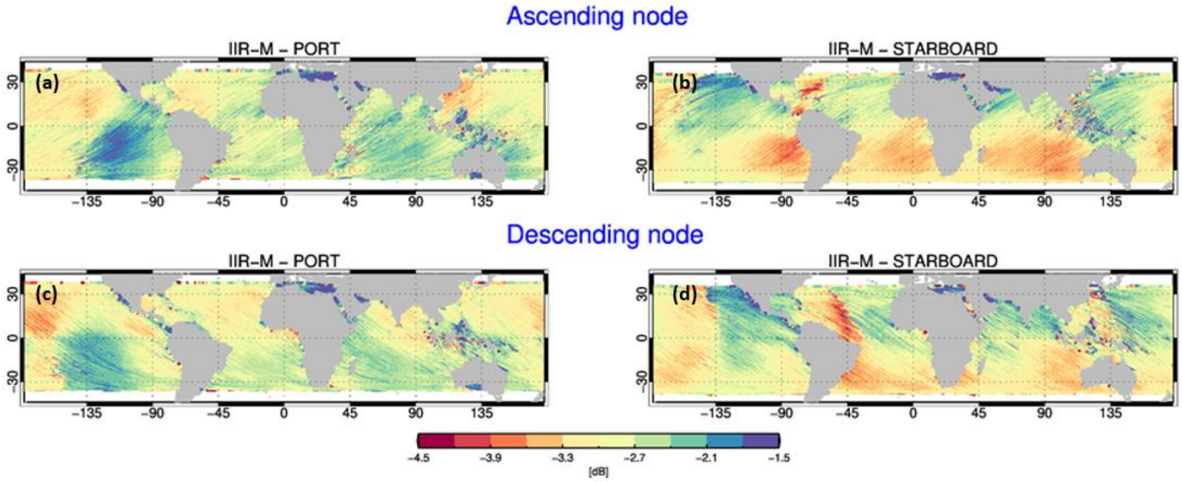

Figure 4-5 Track-wise σ° bias correction for CyGNSS plotted on a map, separated by CyGNSS antenna for block IIR-M only, for the March 01 2020-November 2020. These plots highlight the changes in bias correction due to the flex power event which began in mid-February 2020.

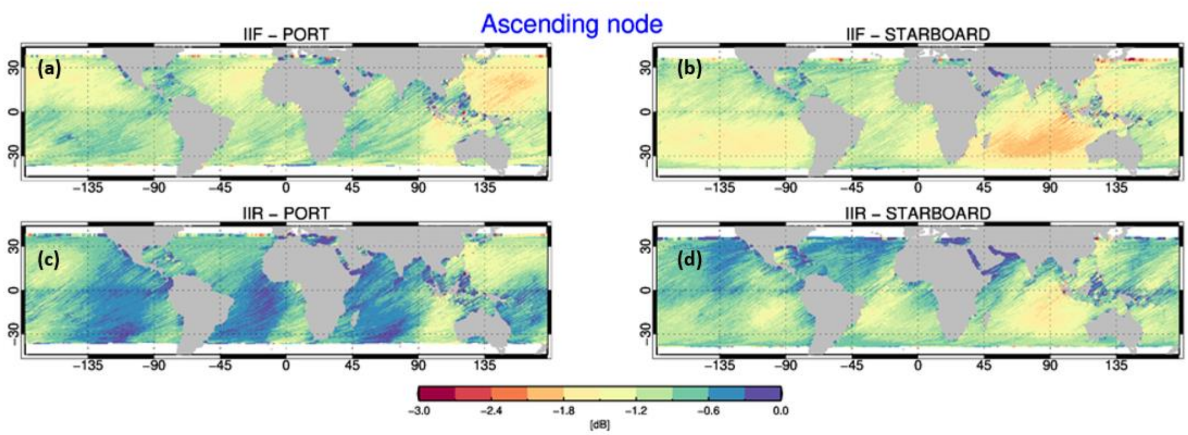

Figure 4-6 Track-wise σ° bias correction for CyGNSS ascending node plotted on a map, separated by CyGNSS antenna for block IIF and IIR, for the March 01 2020-November 2020. Note the change of color bar scale compared to Figure 4-3.

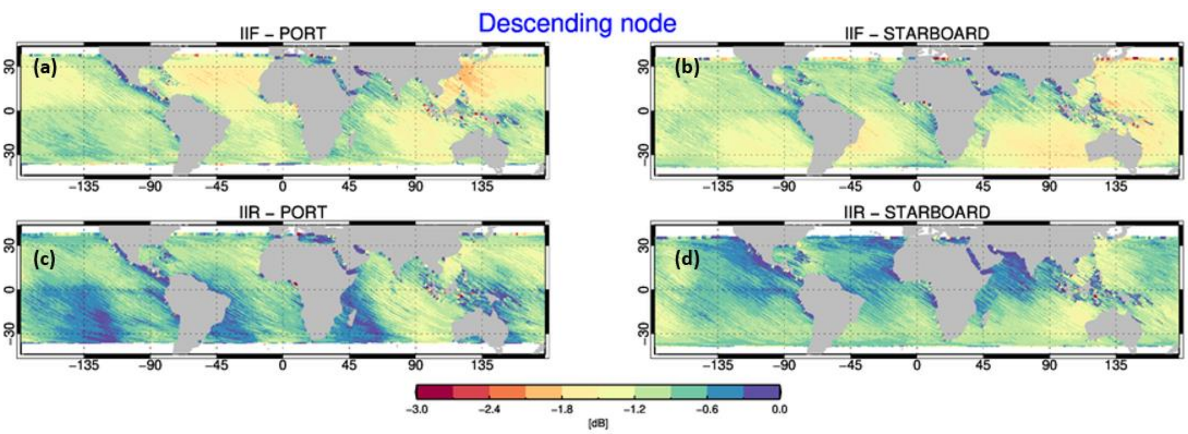

Figure 4-7 Track-wise σ° bias correction for CyGNSS descending node plotted on a map, separated by CyGNSS antenna for block IIF and IIR, for the March 01 2020-November 2020. Note the change of color bar scale compared to Figure 4-4.

4.1.3 Incidence angle dependence plot

According to [3], theoretical σ° dependence to the incidence angle, given a fixed wind speed, monotonically decreases as the incidence angle increases. Figure 4-8 reports CyGNSS binned averaged σ° for a given wind speed bin (6-6.5 m/s) as a function of incidence angle, separated by CyGNSS antenna and spacecraft number. Plots a, c, e, and g show such data without track-wise bias correction for all block types combined, then for block IIF only, IIR-M only, and IIR only, respectively. The corresponding plots, with track-wise bias correction are found in plots b, d, f, and h. Noticeable intersatellite σ° biases are present in plots a, c, e, and g, including biases between block types. The σ° dependence to the incidence angle does not reflect what the theory predicts either. Applying the track-wise bias correction (see plots b, d, f, and h) removes the intersatellite σ° bias, including biases between block types, but maintains a non-monotonically decreasing trend versus incidence angle.
Figure 4-9 reports CyGNSS binned averaged σ° bias (i.e. measured-predicted) as a function of incidence angle, separated by CyGNSS antenna and spacecraft number. Plots a, c, e, and g show such data without track-wise bias correction for all block types, for block IIF, IIR-M, and IIR, respectively. The corresponding plots, with track-wise bias correction are found in plots b, d, f, and h. Again, similar observations are made as from Figure 4-8, that is the presence of intersatellite σ° biases, biases between a given spacecraft CyGNSS antennas, and between block types. Once again, applying the track-wise bias correction removes these unwanted calibration issues, while leaving a residual absolute bias of ~ 0.05-.1 dB.

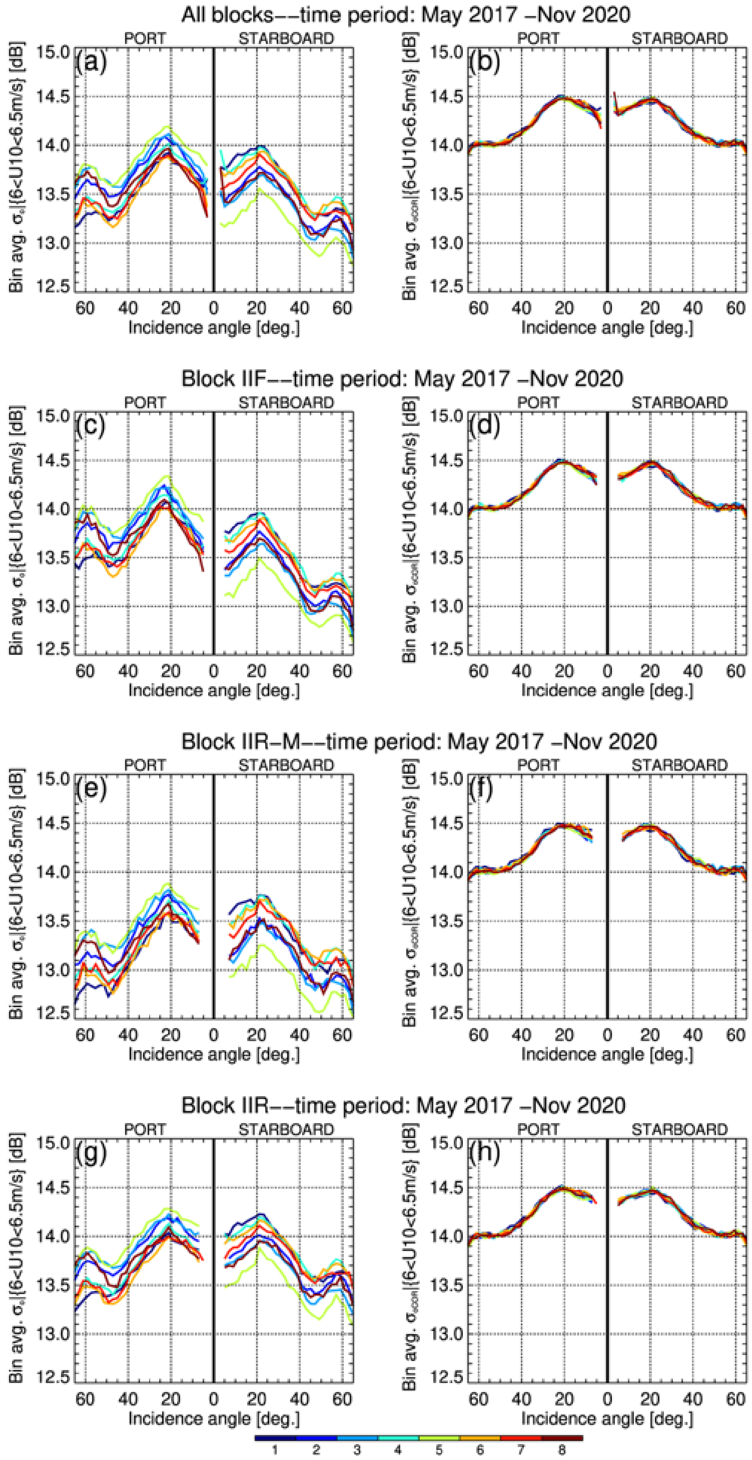

Figure 4-8 Binned averaged σ°, given a wind speed between 6-6.5 m/s, separated by CyGNSS antenna, spacecraft number, without track-wise bias correction, for all GPS block type combined (see plot a), for block IIF only (see plot c), block IIR-M (see plot e), and block IIR (see plot g). Corresponding plots with the track-wise bias correction applied are shown in plots b, d, f, and h.

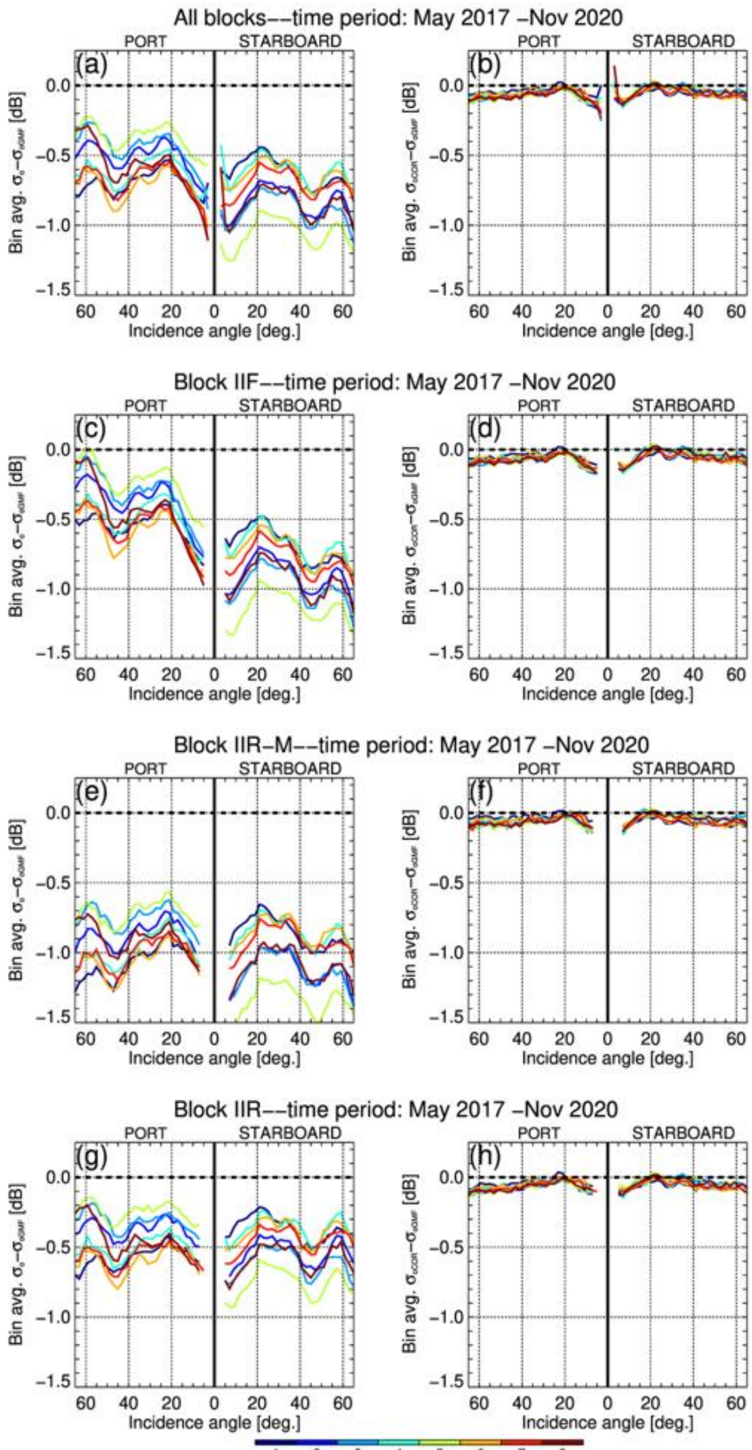

Figure 4-9 Binned averaged σ° bias (i.e. measured-predicted) separated by CyGNSS antenna, spacecraft number, without track-wise bias correction, for all GPS block type combined (see plot a), for block IIF only (see plot c), block IIR-M (see plot e), and block IIR (see plot g). Corresponding plots with the track-wise bias correction applied are shown in plots b, d, f, and h.

4.2 Wind speed domain analysis

4.2.1 Global analysis against ECMWF

A global wind speed analysis is now shown using ¼ degree ECMWF winds bi-linearly interpolated in space and time to v1.2 NOAA CyGNSS winds. The selected time period is May 2017 to December 2021. Figure 4-10 reports geographical distributions of the collocated data (see plot (a)), the wind speed error between CyGNSS and ECMWF (see plot (b)), and the standard deviation of the error (see plot (c)). As can be seen from plot (b), higher wind speed errors are first associated with the Intertropical Convergence Zone (ITCZ); this is no surprise as we expect model winds to struggle in such region due to the frequency and unpredictability of convective events. Other regions of the globe, such as east of the south American continent, southern tip of Africa, and the north western Pacific Ocean, exhibit larger positive wind speed biases where CyGNSS winds are reportedly higher than ECMWF. After further investigations, these regions are primarily associated with a higher probability of high wind, in which case CyGNSS would report higher wind than ECMWF. Similarly, regions with higher standard deviation of the error (stde), as shown in Figure 4-10c, are mostly associated with regions with high wind probability. However, there are still other sources which can contribute to higher stde which have yet to be identified.

Figure 4-11a provides a 2-D histograms of CyGNSS versus ECMWF winds. The overall bias is 0.18 m/s with a stde of 1.15 m/s computed from more than 452 million samples. A closer look at the scatterplot first shows the absence of outliers (i.e. high CyGNSS wind speed samples collocated with low ECMWF wind speed samples), thanks to the improved version of the quality flag. Second, this plot shows CyGNSS tendency to overestimate winds, compared to ECMWF, when the latter is greater than 15 m/s. This is by design as it is well known that model prediction winds, such as ECMWF, tend to underestimate the wind speed within the high wind regime.

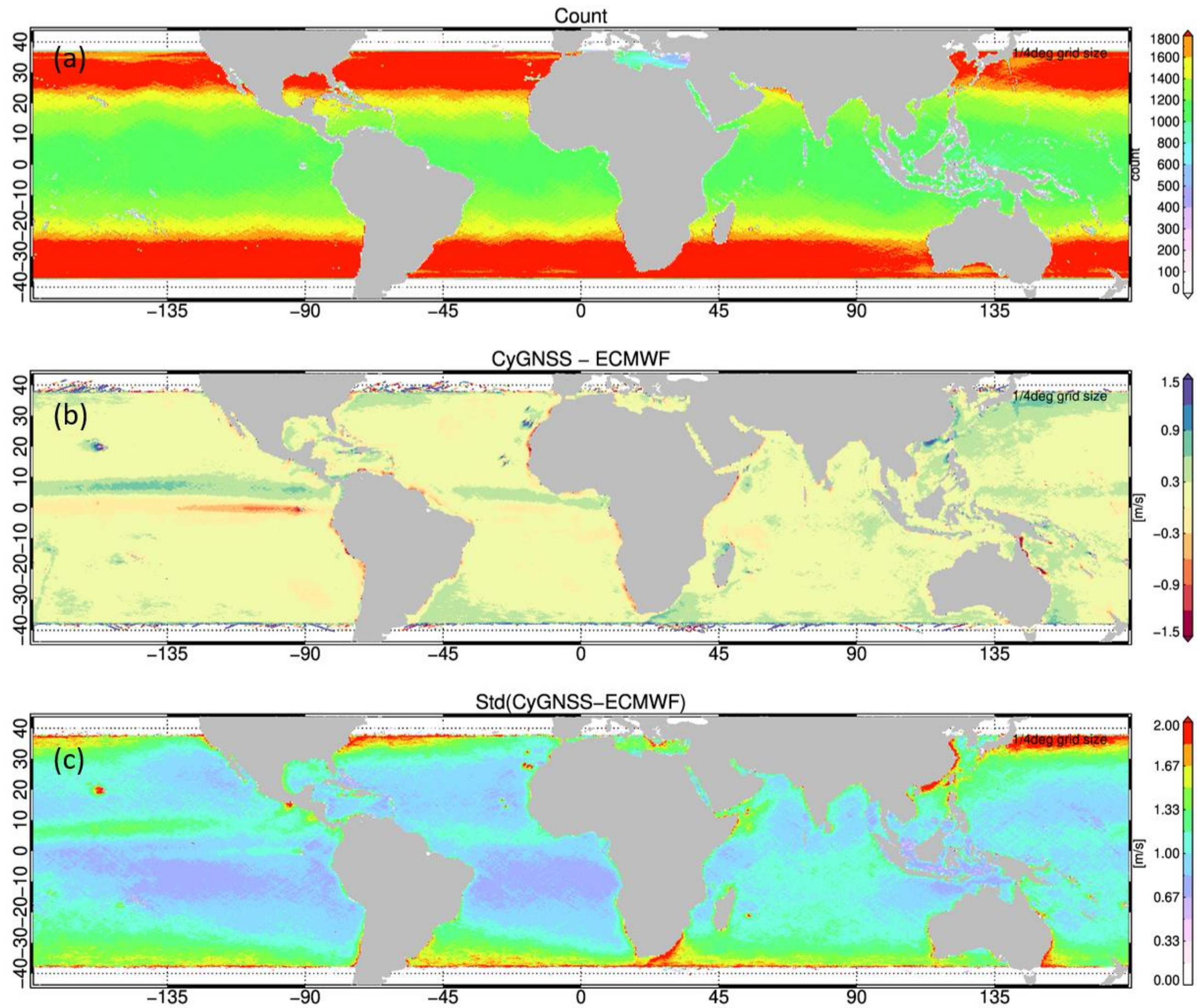

Figure 4-10 Geographical distributions of CyGNSS wind speed samples (see plot (a)), wind speed error between CyGNSS and ECMWF (see plot (b)), and the standard deviation of the wind speed error (see plot (c)). Bin size used for the generation of these plots is a ¼ degree.

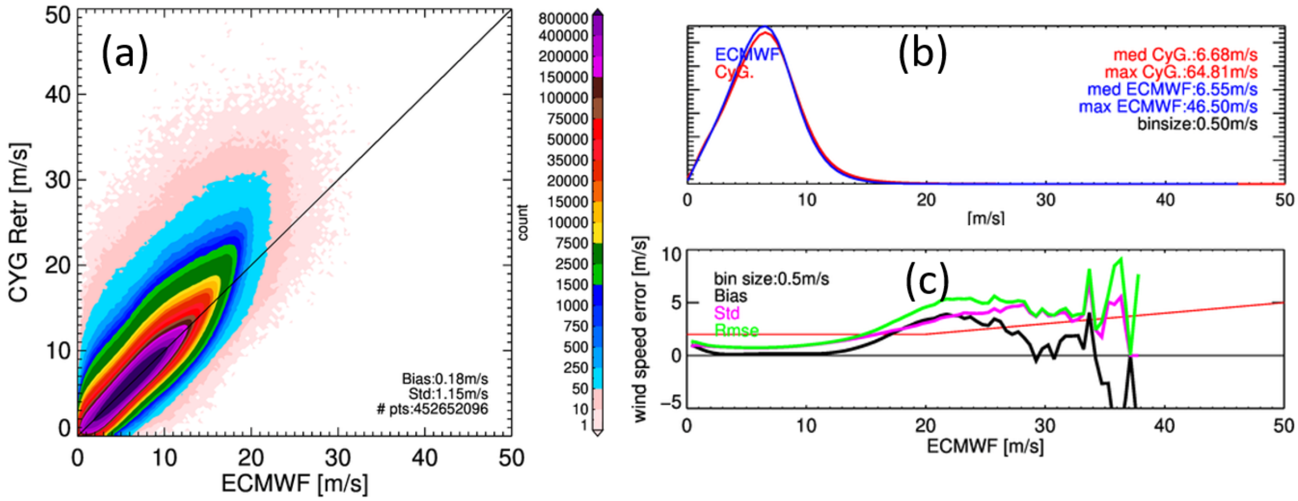

Figure 4-11 2-D histogram of CyGNSS vs. ECMWF winds (see plot (a)), and their corresponding histograms (see plot (b)). Plot (c) shows the wind speed error (i.e. CyGNSS-ECMWF), the standard deviation of the error, and the RMSE as a function ECMWF.

4.2.2 High wind performance

1-2 km high resolution HWRF data, regridded to a ¼ degree resolution, is used to assess v1.2 NOAA CyGNSS wind performance in the high wind regime. Just like with ECMWF, HWRF data is bilinearly interpolated in space and time to CyGNSS wind data. The selected time period is also May 2017 to December 2021.

Figure 4-12 reports geographical distributions of the collocated data (see plot (a)), the wind speed error between CyGNSS and HWRF (see plot (b)), and the standard deviation of the error (see plot (c)). In general, the wind speed error mostly remains between -1 to 1 m/s within the Atlantic and eastern Pacific basins. Areas where the error is noticeably higher are usually associated to areas with low sample count (i.e. compare plot (b) with plot (a)).

Figure 4-13a shows a 2-D histogram of CyGNSS versus HWRF winds. The overall bias is 0.15 m/s with a stde of 2.50 m/s computed from more than 1 million samples. The scatterplot shows a good agreement overall between CyGNSS and HWRF where the overall scatter remains symmetrical about the one-to-one line. The scatter slowly increases, however, as HWRF wind speed is increasing. Figure 4-13b reports a good agreement between their respective histograms. Finally, the stde remains below the mission requirement up to ~18 m/s (i.e. see intersection of magenta curve with red curve on Figure 4-13c).

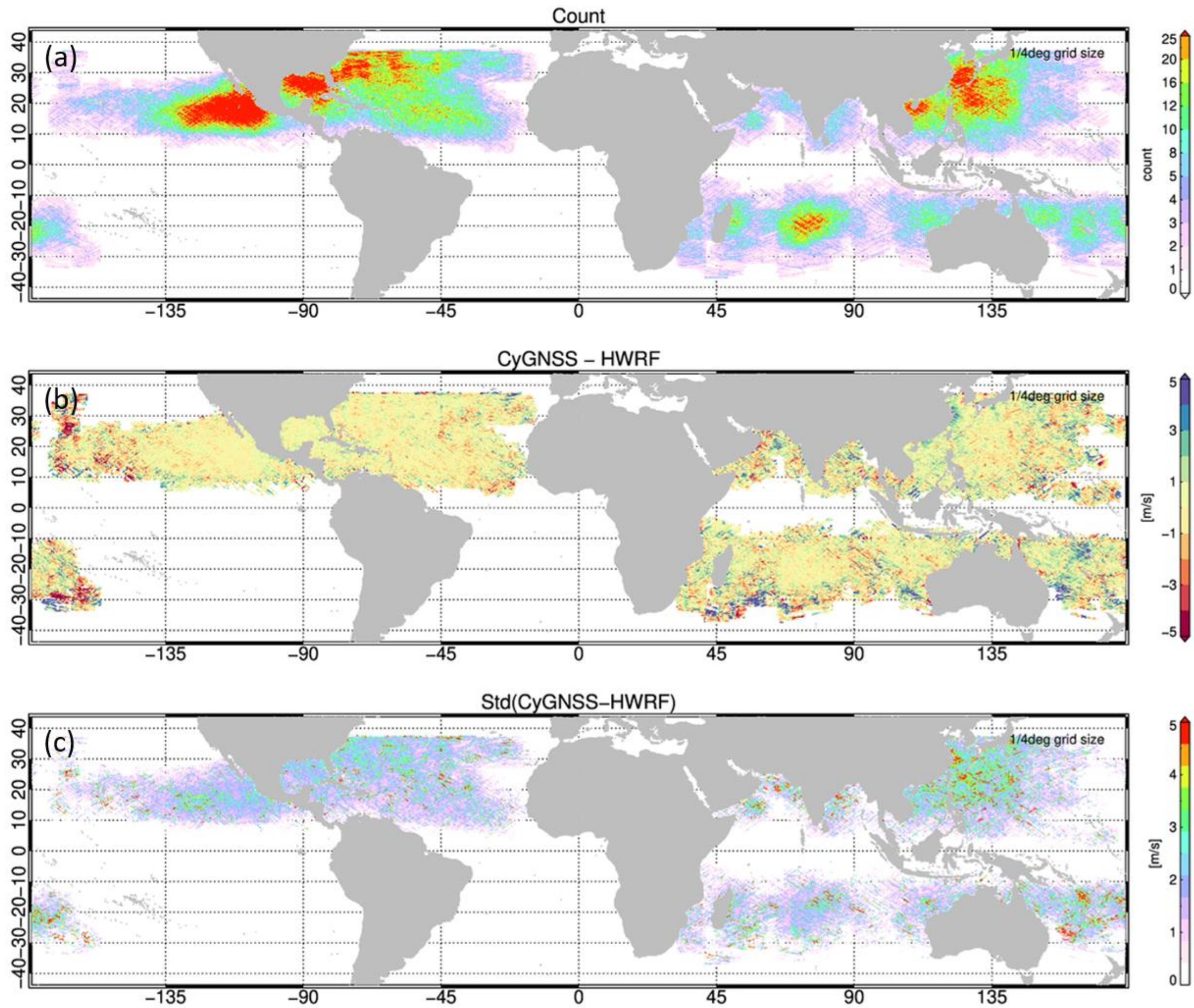

Figure 4-12 Geographical distributions of CyGNSS wind speed samples (see plot (a)), wind speed error between CyGNSS and HWRF (see plot (b)), and the standard deviation of the wind speed error (see plot (c)). Bin size used for the generation of these plots is a ¼ degree.

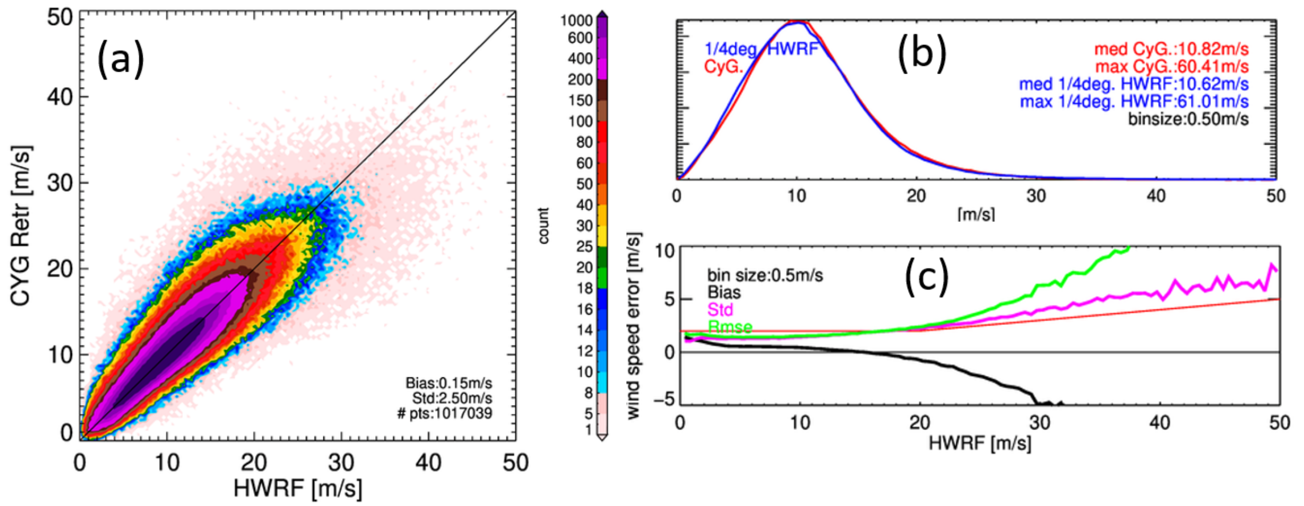

Figure 4-13 2-D histogram of CyGNSS vs. HWRF winds (see plot (a)), and their corresponding histograms (see plot (b)). Plot c shows the wind speed error (i.e. CyGNSS-HWRF), the standard deviation of the error, and the RMSE as a function HWRF.

5 Data access

This section provides useful information regarding data file content, the use of the provided quality flag, a description of the wind speed sample error characterization, and finally data file availability.

5.1 Data description

The NOAA Level 2 CyGNSS data is saved in NetCDF file format. Each file contains data from up to eight CyGNSS spacecraft, covering a period of 24 hours. Table 1 provides detailed information about the variables that are found within each NetCDF file.

Table 1 List of variables found in NOAA Level 2 CyGNSS NetCDF files

Name	Description	Data type	Dimension
sample	Sample index	Long	grid(ysize)
spacecraft_num	CyGNSS spacecraft number	Byte	grid(ysize)
prn_code	GPS PRN code	Byte	grid(ysize)
sv_num	GPS space vehicle number	Long	grid(ysize)
antenna	Receive antenna	Byte	grid(ysize)
sample_time	Sample time	Double	grid(ysize)
lat	Latitude	Float	grid(ysize)
lon	Longitude	Float	grid(ysize)

sc_lat	Subsatellite point latitude	Float	grid(ysize)
sc_lon	Subsatellite point longitude	Float	grid(ysize)
incidence_angle	Incidence angle	Float	grid(ysize)
track_id	Track ID	Long	grid(ysize)
rx_gain	Rx antenna gain	Float	grid(ysize)
snr	Signal-to-noise ratio	Float	grid(ysize)
range_corr_gain	Range corrected gain	Float	grid(ysize)
sample_flags	Status flags for the sample	Long	grid(ysize)
num_ddms_utilized	Number of DDMs utilized	Byte	grid(ysize)
ddm_sample_index	Level 1 NetCDF sample indices	Long	grid(xsize,ysize)
ddm_channel	Level 1 DDM reflectometry channel	Long	grid(xsize,ysize)
nbrcs_mean	Normalized BRCS averaged in a 25x25km grid cell	Float	grid(ysize)
nbrcs_mean_corrected	Corrected normalized BRCS averaged in a 25x25km grid cell	Float	grid(ysize)
wind_speed	Retrieved wind speed	Float	grid(ysize)
wind_speed_uncertainty	Retrieved wind speed error	Float	grid(ysize)
azimuth_angle	Azimuth angle	Float	grid(ysize)
sc_roll	Spacecraft attitude roll angle	Float	grid(ysize)
sc_pitch	Spacecraft attitude pitch angle	Float	grid(ysize)
sc_yaw	Spacecraft attitude yaw angle	Float	grid(ysize)
sc_alt	Spacecraft altitude	Float	grid(ysize)

5.2 Quality Flag

A quality flag variable (named ‘sample_flags’ – see Table 1) is provided so as to help users filter out poor quality samples and/or select specific data subset (e.g. retrieve wind speed samples for a specific satellite orbital node). The ‘sample_flags’ variable unit is a bit field. In this current version (v1.2) of the data product, eight separate bits (starting at bit 0) are currently used. Table 2 shows the list of bits with their respective description.

Table 2 ‘Sample_flags’ bit description

Bit flag	value	description
0	0	data is considered of ‘good quality’
	1	data is considered of ‘poor quality’. This is the result of the logical OR of: bit 6 being ‘set’, bit 7 being ‘set’.
1	0	descending node
	1	ascending node
2	0	data from GPS blocks IIR and IIRM
	1	data from GPS block IIF only
3	0	data from GPS blocks IIF and IIRM
	1	data from GPS block IIR only
4	0	data from GPS blocks IIR and IIF
	1	data from GPS block IIR-M only
5	0	the Level 1 "nst_att_status" flag (i.e. related to the nano star tracker) is zero
	1	the Level 1 "nst_att_status" flag is nonzero
6	0	wind speed quality OK WHILE the nano star tracker flag (i.e. nst_att_status) is set
	1	low confidence in the reported wind speed WHILE the nano star tracker flag is set.
7	0	free of unrealistic wind speed samples
	1	unrealistic wind speed samples detected

Equation (1) shows how to filter out the ‘poor quality samples’ (i.e. bit 0) using the modulo operator such that

$$MOD\left(\frac{\text{long(sample\_flags)}}{2^0}, 2\right) = 0. \tag{1}$$

Whenever Equation (1) is true, the wind speed samples are considered of good quality. Note the exponent in the denominator of the modulo operand: a '0' is used because bit 0 represents the poor overall quality flag bit. Similarly, if one is interested in plotting all available ascending data, then this exponent would be replaced with a '1' and Equation (1) would be set equal to 1. As an illustration, Figure 5-1 shows an ascending and descending passes of NOAA CyGNSS winds on 2020 August 04, with poor quality samples filtered out using Equation (1).

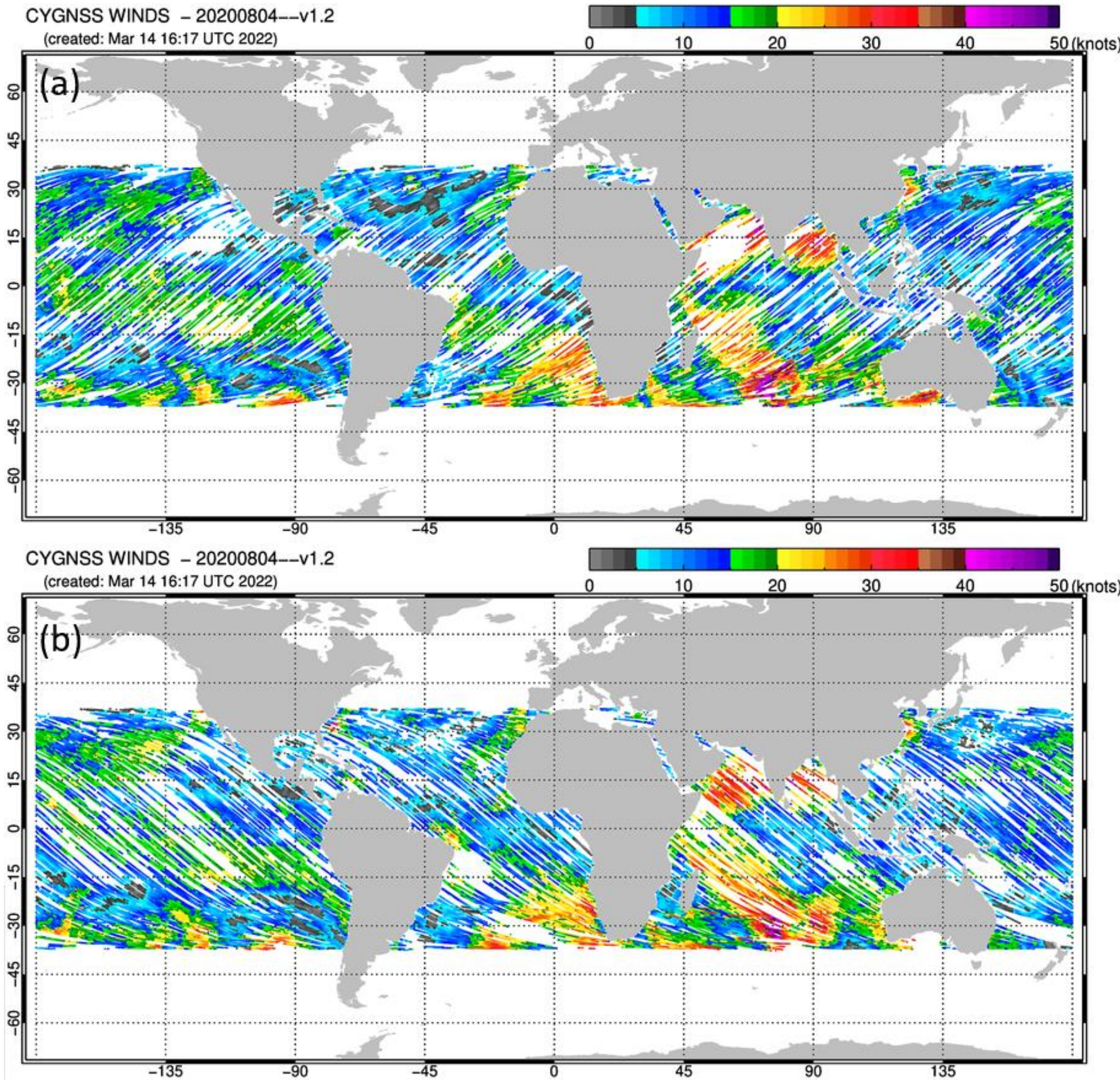

Figure 5-1 Ascending (top) and descending (bottom) passes from all eight CyGNSS spacecraft, showing global retrieved winds for a 24hr period on 2020 August 04.

5.3 Wind sample error characterization

A wind speed sample error variable is now provided. It is derived using the standard deviation of the wind speed error (stde) between CyGNSS and ECMWF. Collocated data from May 2017 until November 2020 was used to generate this metric. Figure 5-2 shows the stde as a function of the retrieved CyGNSS wind. As can be seen, a custom fit was implemented in the higher wind regime to address the noisiness of the curve.

Assigning the error to a wind speed sample first consists of using the relationship between the stde and CyGNSS wind speed, as shown in Figure 5-2, then assigning the corresponding stde to the retrieved wind speed using a straightforward interpolation scheme.

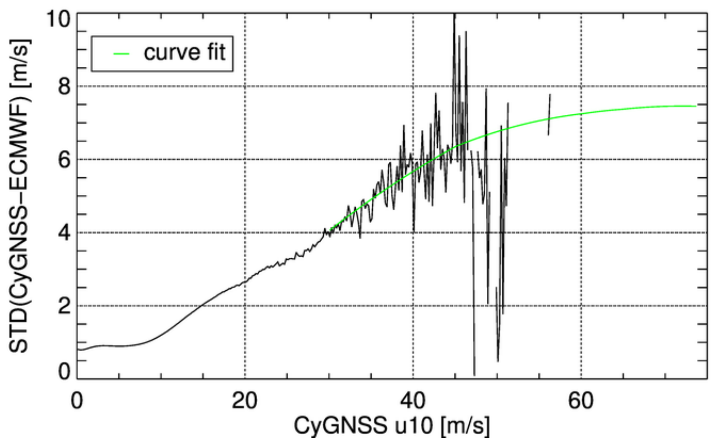

Figure 5-2 Wind speed error curve as a function of CyGNSS retrieved wind speed. A 0.2 m/s bin size was used to generate this curve. Data period is May 2017 to November 2020. The green curve represents a fit to the higher wind speed regime where collocated data is scarce.

5.4 Data file availability

Although the CyGNSS Level 1 data files have been made available to the public since March 18 2017, all eight instrument noise floors were noticeably high until mid to end of April 2017, as shown in Figures 10 and 11 from [6]. As a result, the NOAA Level 2 CyGNSS winds are made available starting May 01 2017.

As previously mentioned, each NetCDF file contains global daily coverage from all eight CyGNSS spacecraft spanning a time period of up to 24 hours. In normal circumstances, there should be a NetCDF file available for each day of year. However, in very rare cases, files may be unavailable for an entire day if numerical weather model prediction data is missing. It is worth noting that if only one spacecraft has its data entirely flagged on a specific day, a NetCDF file will still be made available for that day since it will include valid data for the remaining seven spacecraft.

Finally, once the data is collected from all operating spacecraft for a given day, a NetCDF file is then created and pushed from the NOAA servers to the PO.DAAC.

6 List of references

The following references provide important background information regarding this product including the motivation behind its creation. We invite the users to read these documents. Questions are welcome and can be sent to the authors of this ATBD.

[1] F. Said, Z. Jelenak, J. Park, P. S. Chang and S. Soisuvarn, "NOAA CyGNSS Wind Product - Ver 1.0," OWST, College Park, 2019.

[2] F. Said, Z. Jelenak, J. Park, Q. Zhu and P. S. Chang, "An Overview of NOAA CYGNSS Wind Product Version 1.0," in *IGARSS 2020*, Waikoloa, 2020.

[3] C. Ruf, P. Chang, M. P. Clarizia, S. Gleason, Z. Jelenak, J. Murray, M. Morris and S. Musko, CYGNSS Handbook, 2016.

[4] CYGNSS, *CYGNSS Level 1 Science Data Record Version 2.1. Ver. 2.1.,* PO.DAAC, 2018.

[5] F. Said, Z. Jelenak, J. Park and S. P. Chang, "The NOAA track-wise wind retrieval algorithm and product assessment for CyGNSS," *IEEE Transaction on Geoscience and Remote Sensing,* 2021.

[6] F. Said, Z. Jelenak, P. S. Chang and S. Soisuvarn, "An assessment of CyGNSS normalized radar cross section calibration," *IEEE Journal of Selected Topics in Applied Earth Observations and Remote Sensing,* pp. 50-65, 2019.

[7] N. Rascle and F. Ardhuin, "A global wave parameter database for geophysical applications. Part 2: Model validation with improved source term parameterization," *Ocean Modeling,* vol. 70, 2013.

[8] S. Gleason, S. C. Ruf, J. A. O'Brien and S. D. McKague, "The CYGNSS level 1 calibration algorithm and error analysis based on on-orbit measurements," *IEEE Journal Selected Topics Applied Earth Observing Remote Sensing,* vol. 12, no. 1, pp. 37-49, 2019.

[9] P. Steigenberger, S. Thöler and O. Montenbruck, "Flex power on GPS Block IIR-M and IIF," *GPS Solut,* p. 23, 2019.

[10] P. Steingenberger and A. E, "The New Flex Power Mode:From GPS IIR-M and IIF Satellites With Extended Coverage Area," 21 May 2020. [Online]. Available: https://insidegnss.com/the-new-flex-power-mode-from-gps-iir-m-and-iif-satellites-with-extended-coverage-area/. [Accessed 29 October 2021].

[11] F. Said, Z. Jelenak, J. Park, S. Soisuvarn and P. S. Chang, "Latest cal/val assessment of v2.1 L1/L2 data," OSWT, College Park, 2019.

[12] F. Said, Z. Jelenak, P. S. Chang and J. Park, "An introduction to v1.1 NOAA CyGNSS Wind Product and a look at v3.0 Level 1 data," OSWT, College Park, 2020.

[13] F. Said, Z. Jelenak, J. Park, S. Soisuvarn and P. S. Chang, "First Look at NOAA CyGNSS winds in the Tropical Cyclone Environment," IEEE GNSS+R 2019, Benevento, 2019.

END OF DOCUMENT